Adsorption (2011) 17: 27–38
DOI 10.1007/s10450-010-9268-4

Single component and binary diffusion of n-heptane and toluene in SBA-15 materials

Qinglin Huang · Ramil Abu Qamar · Mladen Eić

Received: 13 May 2010 / Accepted: 14 September 2010 / Published online: 21 October 2010

Abstract In this work, the diffusion properties of single component n-heptane and toluene as well as their binary mixtures in two SBA-15 samples with different structural characteristics were studied by the standard Zero Length Column (ZLC) technique under three different concentration levels. A theoretical ZLC desorption model considering the Generalized Maxwell-Stefan (GMS) formulation was developed. Using the independently measured single component equilibrium and kinetic parameters, the model was able to reasonably predict experimental binary ZLC desorption curve for countercurrent diffusion of toluene in the presence of n-heptane. However, there was a significant deviation between model prediction results and experimental data for countercurrent desorption of n-heptane in the presence of toluene. The diffusion of n-heptane is reduced by the presence of toluene, regardless of the relative content of micropores in the intrawall pores, while that of toluene is virtually unaffected by the counter-diffusion of n-heptane. The observed phenomena cannot be addressed by the simple model considering the cross term diffusion effect. The structural property of material and the molecular characteristics of probe molecules were used to account for the difference in the behavior between n-heptane and toluene.

Keywords SBA-15 · Binary diffusion · n-Heptane · Toluene · ZLC technique

Q. Huang · R.A. Qamar · M. Eić (✉)
Department of Chemical Engineering, University of New Brunswick, P.O. Box 4400, Fredericton, NB E3B 5A3, Canada
e-mail: meic@unb.ca

1 Introduction

SBA-15 is silica material consisting of two-dimensional hexagonal arrays of mesoporous channels that typically range from 4–10 nm in diameter. Due to its appealing textural properties, such as high specific surface area, as well as appreciable thermal and hydrothermal stability, SBA-15 has attracted great research interests in adsorption, catalysis, and chromatography since its first introduction in 1998 (Zhao et al. 1998, 2002; Newalkar et al. 2002; Rioux et al. 2005; Vinh-Thang et al. 2005a). Several studies dealing with SBA-15 materials revealed the presence of irregular intrawall pores with a broad distribution in the micropore/small-mesopore range within the pore walls of the mesoporous structure (Kruk et al. 2000; Ravikovitch and Neimark 2001; Sun et al. 2003; Galarneau et al. 2003; Choi et al. 2003; Vinh-Thang et al. 2005b). The open ended fraction of intrawall pores are considered responsible for interconnecting adjacent primary mesopore channels.

Studying the roles of micropore and mesopore on the mechanisms as well as transport properties of sorbate molecules in the SBA-15 materials is an essential first step in developing novel materials for potential applications. In our previous studies (Vinh-Thang et al. 2005b, 2006a), diffusion of single component n-heptane, cumene and mesitylene in a series of bi-porous (micro- and mesoporous) SBA-15 materials was investigated by the Zero Length Column (ZLC) technique at a low concentration level. Intrawall pores were found to play a major role in controlling diffusion. The overall diffusion process of probe molecules is controlled by a combination of micro- and mesopore-diffusion resistances in the mesoporous walls and depends on the relative content of micropores.

Since many typical industrial processes, such as adsorption separation and catalytic reaction usually involve more

than one component, the knowledge of multicomponent diffusion is required for exploring SBA-15 materials in the potential applications. To date such analysis in SBA-15 materials has not been reported in the literature yet. Furthermore, ZLC technique has been widely used to investigate single component diffusion in many different systems since it was developed in the late 1980s (Eić and Ruthven 1988). However, study of multicomponent diffusion using ZLC technique has been rather limited (Brandani et al. 2000a, 2000b). The aim of this work is to apply this technique to investigate single component n-heptane and toluene as well as their binary mixture in two SBA-15 samples under three different concentration levels.

2 Theory

The development of ZLC models was based on these assumptions: (a) the system was considered isothermal; (b) there was no external film resistance to gas transport; (c) the gas hold-up in the fluid phase was neglected in comparison with the adsorbed phase accumulation.

Subject to these assumptions, fluid phase mass balance in the ZLC column is given by,

$$v_s \frac{d\bar{q}_i}{dt} + F(c_i - c_i^{\text{in}}) = 0 \tag{1}$$

where v_s is volume of adsorbent particles assumed to be spherical; F is purge flow rate; c_i and c_i^{in} are outlet and inlet fluid phase concentrations across the ZLC column for component i; $\bar{q}_i$ is the average adsorbed phase concentration for component i, which is related to the adsorbate flux at the particle surface by the following equation:

$$\frac{d\bar{q}_i}{dt} = \frac{3}{R} D_i \frac{\partial q_i}{\partial r}\bigg|_{r=R} \tag{2}$$

where D_i is the effective diffusivity, which is presumed to be constant in the linear adsorption isotherm range and concentration dependent outside the linear range, and R is particle radius.

Combining (1) and (2), the mass balance around particle surface is obtained,

$$D_i \frac{\partial q_i}{\partial r}\bigg|_{r=R} + \frac{FR}{3v_s}(c_i|_{r=R} - c_i^{\text{in}}) = 0 \tag{3}$$

The mass balance equation inside the adsorbent particle is given by,

$$\frac{\partial q_i}{\partial t} = \frac{1}{r^2}\frac{\partial}{\partial r}\left(D_i r^2 \frac{\partial q_i}{\partial r}\right) \tag{4}$$

For a linear equilibrium and single component system, c_i^{in} is zero and mathematical expression of normalized effluent sorbate concentration is given by Eić and Ruthven (1988),

$$\frac{c_i}{c_{oi}} = 2L \sum_{n=1}^{\infty} \frac{\exp(-\beta_n^2 D_{oi} t/R^2)}{[\beta_n^2 + L(L-1)]} \tag{5}$$

where D_{oi} is the limiting diffusivity of component i; β_n are eigen-values given by the roots of the auxiliary equation,

$$\beta_n \cot \beta_n + L - 1 = 0 \tag{6}$$

and

$$L = \frac{FR^2}{3K v_s D_{oi}} \tag{7}$$

where K is Henry's constant. For the long time solution (5) is reduced to simple exponential decay curves since only the first term of the summation is significant,

$$\frac{c_i}{c_{oi}} = 2L \frac{\exp(\frac{-\beta_1^2 D_{oi} t}{R^2})}{\beta_1^2 + L(L-1)} \tag{8}$$

For a single component (c_i^{in} is zero) and nonlinear equilibrium following the Langmuir adsorption isotherm system, the gas phase concentration around particle surface in (3) is represented by,

$$c_i|_{r=R} = \frac{\theta_i}{b_i(1-\theta_i)}\bigg|_{r=R} \tag{9}$$

and D_i in (3) and (4) can be obtained from Generalized Maxwell-Stefan (GMS) theory (Krishna 1993). D_i is concentration dependent and follows the commonly known Darken's equation,

$$D_i = D_{oi} \frac{1}{1-\theta_i} \tag{10}$$

where θ_i $(= q_i/q_s)$ is fractional coverage of adsorption sites; b_i and q_s are Langmuir equilibrium parameters.

For a binary (components A and B) nonlinear adsorption equilibrium system, the gas phase and adsorbed phase concentration around particle surface is assumed to comply with the extended Langmuir model,

$$\left.\begin{aligned} c_A|_{r=R} &= \frac{\theta_A}{b_A(1-\theta_A-\theta_B)}\bigg|_{r=R} \\ c_B|_{r=R} &= \frac{\theta_B}{b_B(1-\theta_A-\theta_B)}\bigg|_{r=R} \end{aligned}\right\} \tag{11}$$

D_i in (3) and (4) has the following expressions (Round et al. 1966),

$$\left.\begin{aligned} D_A &= D_{AA} + D_{AB}\frac{\partial q_B/\partial r}{\partial q_A/\partial r} \\ D_B &= D_{BB} + D_{BA}\frac{\partial q_A/\partial r}{\partial q_B/\partial r} \end{aligned}\right\} \tag{12}$$

where D_{AA}, D_{BB} are straight diffusivities and D_{AB}, D_{BA} are cross diffusivities, which are derived according to GMS theory (Krishna 1993), assuming a binary Langmuir system:

$$\left.\begin{aligned} D_{AA} &= \frac{(D_0)_A(D_0)_B\left(\frac{1-\theta_B}{(D_0)_B} + \frac{\theta_A}{(D_0)_{BA}}\right)}{(1-\theta_A-\theta_B)\left(1 + \frac{\theta_B(D_0)_A}{(D_0)_{AB}} + \frac{\theta_A(D_0)_B}{(D_0)_{BA}}\right)}, \\ D_{AB} &= \frac{(D_0)_A(D_0)_B\theta_A\left(\frac{1}{(D_0)_B} + \frac{1}{(D_0)_{AB}}\right)}{(1-\theta_A-\theta_B)\left(1 + \frac{\theta_B(D_0)_A}{(D_0)_{AB}} + \frac{\theta_A(D_0)_B}{(D_0)_{BA}}\right)} \\ D_{BA} &= \frac{(D_0)_A(D_0)_B\theta_B\left(\frac{1}{(D_0)_A} + \frac{1}{(D_0)_{AB}}\right)}{(1-\theta_A-\theta_B)\left(1 + \frac{\theta_B(D_0)_A}{(D_0)_{AB}} + \frac{\theta_A(D_0)_B}{(D_0)_{BA}}\right)}, \\ D_{BB} &= \frac{(D_0)_A(D_0)_B\left(\frac{1-\theta_A}{(D_0)_A} + \frac{\theta_B}{(D_0)_{BA}}\right)}{(1-\theta_A-\theta_B)\left(1 + \frac{\theta_B(D_0)_A}{(D_0)_{AB}} + \frac{\theta_A(D_0)_B}{(D_0)_{BA}}\right)} \end{aligned}\right\} \tag{13}$$

where $(D_0)_A$ and $(D_0)_B$ are the limiting diffusivities of components A and B, respectively; $(D_0)_{AB}$ and $(D_0)_{BA}$ are limiting cross diffusivities, which can be estimated by the empirical Vignes correlation (Vignes 1966),

$$(D_0)_{AB} = (D_0)_{BA} = [(D_0)_A]^{\theta_A/(\theta_A+\theta_B)}[(D_0)_B]^{\theta_B/(\theta_A+\theta_B)} \tag{14}$$

Hence, (3), (4), (9), (10), and (3), (4), (11)–(14) constitute single component and binary ZLC models with nonlinear adsorption equilibrium, respectively. The gas phase concentration profiles at the particle surface yield the corresponding ZLC response curves. The models are solved numerically using gPROMS simulation software.

3 Experimental

3.1 Materials and structural characterization

Two SBA-15 samples designated as SBA-15-80 and SBA-15-130 (80 and 130 are aging temperatures in °C during sample preparation) were synthesized at Laval University. A detailed account of the synthesis procedures has been reported by Vinh-Thang et al. (2005b).

Nitrogen adsorption/desorption isotherms of SBA-15 samples at 77 K were performed by a high precision automatic constant volume gas adsorption unit (BELSORP-max, BEL JAPAN Inc.), which is designed for adsorption/desorption isotherm measurement for non-corrosive gases and vapors. Prior to measurements samples were degassed at 200°C and 1.0×10^{-4} Pa for 10–12 hours. The specific surface areas (S_{BET}) of the samples were calculated from adsorption isotherm data using the BET method. The mesopore size distribution was determined using the modified Barrett-Joyner-Halenda (BJH) method from adsorption isotherm data (Kruk et al. 1997). In addition the α_s-plots using macroporous silica gel LiChrospher Si-1000 as a reference adsorbent were applied to estimate the micropore volume.

Electron micrographs of SBA-15 samples were obtained from a JEOL JSM6400 scanning electron microscope (SEM) operated at 15 kV to estimate particle size.

3.2 Adsorption equilibrium measurements

Adsorption equilibrium isotherms for n-heptane and toluene in SBA-15 samples were also measured by the constant volume gas adsorption unit (BELSORP-max). The unit basically consisted of dose tubing and sample test cell, which were connected by pneumatic valves controlled with pressurized air. A turbo molecular pump and a diaphragm pump were used for obtaining high vacuum. Adsorptive gas/vapor was introduced into the dose tubing through valves. The system temperature control is essential to successfully apply constant volume method for gas adsorption measurement. Temperature of dose tubing, pressure sensors and valves was maintained at 40°C in an insulated chamber. The sample cells were immersed in a custom-made constant temperature bath to maintain steady temperature at a desired level during measurements. A digital temperature controller (Cole-parmer A-12107-50) within ±0.1°C was used for the purpose. Prior to beginning the experiment, SBA-15 sample placed in the sample cell was regenerated at 200°C under high vacuum (up to 1.0×10^{-4} Pa) for 10–12 hours. The sample was then cooled down to room temperature, and weighed using an analytical balance (0.01 mg readability). High purity hydrocarbon, i.e., n-heptane (99 wt%; Aldrich), or toluene (99 wt%; Aldrich), was filled in a dosing bottle, and then degassed to remove the dissolved gas for at least three times following steps of freezing liquid to solid, vacuum evacuation for 5 minutes and melting solid to liquid. The instrument automatically collected isotherm data of the target setting pressure and experimental points. When pressure change for 500 seconds in sample cell was within 0.3% of pressure during measurement, adsorption/desorption was considered to reach equilibrium.

3.3 ZLC measurements

The ZLC set-up was similar to the one used in our previous study (Vinh-Thang et al. 2005b). The ZLC column

and switching valve were placed in a gas chromatograph oven (Hewlett Packard Series II 5890). The effluent gas stream during ZLC measurement was continuously monitored with a quadrupole mass spectrometer (Dycor Dymaxion Quadrupole MS). The sample (1 to 2 milligrams) was pretreated at 120°C for 5 hours to remove moisture. After cooling down to room temperature, the dry sample was accurately weighed using an analytical balance (0.01 mg sensitivity). The sample was then loaded into the ZLC column and further activated at 200°C overnight by purging with small flow of helium (~10 cm^3/min) to remove any residual impurities. Prior to desorption measurement, the sample was fully equilibrated with n-heptane or toluene diluted in a helium flow at the desired temperature. In the single component ZLC measurements (designated as NZLC), the sorbate concentration was maintained either low (e.g., 0.005–0.01 Torr partial pressure) or high enough to ensure that the measurements were carried out within or outside the linear range of equilibrium isotherm, respectively. The desorption measurements were performed by purging with pure helium at the same flow rate ensuring it is high enough to maintain a very low sorbate concentration at the external surface of the particles, thus minimizing external heat and mass transfer resistances. For NZLC, under linear conditions, essentially the same diffusion parameters were extracted from the experimental runs under various purge flow rates. The NZLC experimental results obtained under non-linear conditions diverged at the different flow rates, if the desorption curves were plotted in the form of $\ln(c/c_0)$ vs. $F{\cdot}t$ (purge volume). This confirmed that the NZLC measurements were carried out under conditions of kinetic control (Brandani et al. 2000c). In the counter-current binary ZLC measurements (designated as CCZLC), the sample was initially saturated with n-heptane or toluene diluted in a helium flow, and then desorbed with helium containing toluene or n-heptane at the same flow rate.

4 Results and discussion

4.1 Structural characterization

The adsorption/desorption isotherms of nitrogen in two SBA-15 samples are shown in Fig. 1(a). The shape of these isotherms conforms to type IV with H_1 hysteresis loops according to IUPAC classification, which is indicative of mesoporous materials. The extent of increase in adsorption capacity at low relative pressures ($P/P_0 < 0.05$), corresponding to monolayer/initial multiplayer adsorption in the intra-wall pores (micropores and secondary mesopores) of samples (Vinh-Thang et al. 2005b), is larger for SBA-15-80 than SBA-15-130. The same trend is observed until the onset of capillary condensation in the primary mesopores. However, the trend becomes different, i.e., SBA-15-80 showing smaller capacity for nitrogen than SBA-15-130, as P/P_0 ratio becomes greater than 0.79. This indicates that SBA-15-80 has both higher intra-wall pore volume and BET surface area, but smaller total pore volume compared to SBA-15-130. Figure 1(b) displays the mesopore size distribution (PSD) curves estimated by the modified BJH method. Primary mesopore (main channel) diameters were determined from the maxima (peaks) of PSD plots. In addition to the narrow distribution of large (primary) mesopores, the SBA-15 samples exhibit some smaller (secondary) mesopores with a broad distribution. Micropore volume was determined from α_s-plot analysis. Table 1 summarizes the structural data of the two samples. As can be seen from the table, the two samples synthesized at different temperatures exhibit different microporosity, mesoporosity and surface area. The micropore volume in SBA-15-130 is much smaller than in SBA-15-80.

4.2 Adsorption equilibrium isotherms of hydrocarbons

The equilibrium isotherms of n-heptane and toluene on the two samples investigated in this study at different temper-

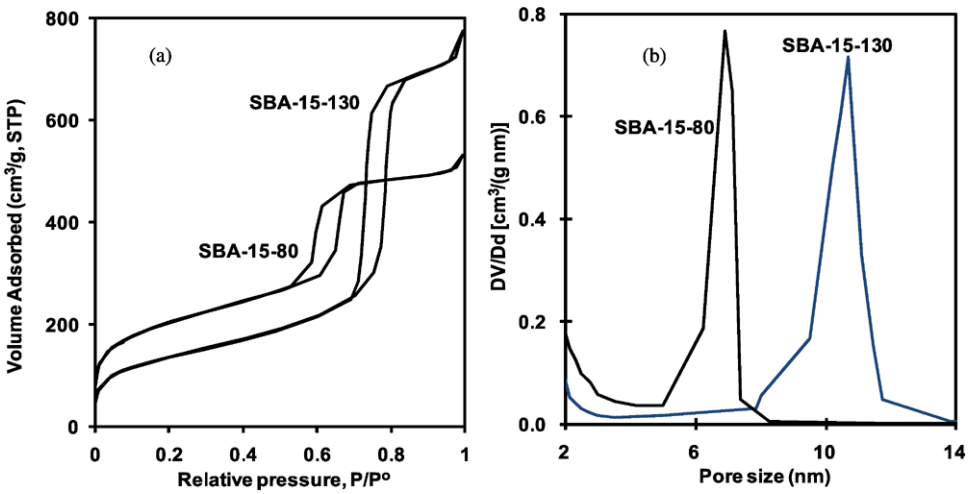

Fig. 1 (**a**) Nitrogen adsorption/desorption isotherms at 77 K and (**b**) pore size distributions from the modified BJH method, for SBA-15-80 and SBA-15-130

Table 1 Textural properties of mesoporous SBA-15 silicas

Sample	S_{BET} (m^2/g)	Total pore volume, v_t from $P/P_0 = 0.99$ (cm^3/g)	Micropore volume from α_s-plot (cm^3/g)	Secondary mesopore volume (cm^3/g)	Primary mesopore volume (cm^3/g)[a]	Primary mesopore diameter (nm)
SBA-15-80	732	0.82	0.07	0.17	0.58	6.9
SBA-15-130	493	1.20	0.01	0.06	1.13	10.7

[a]Primary mesopore volume = total pore volume − micropore volume − secondary mesopore volume

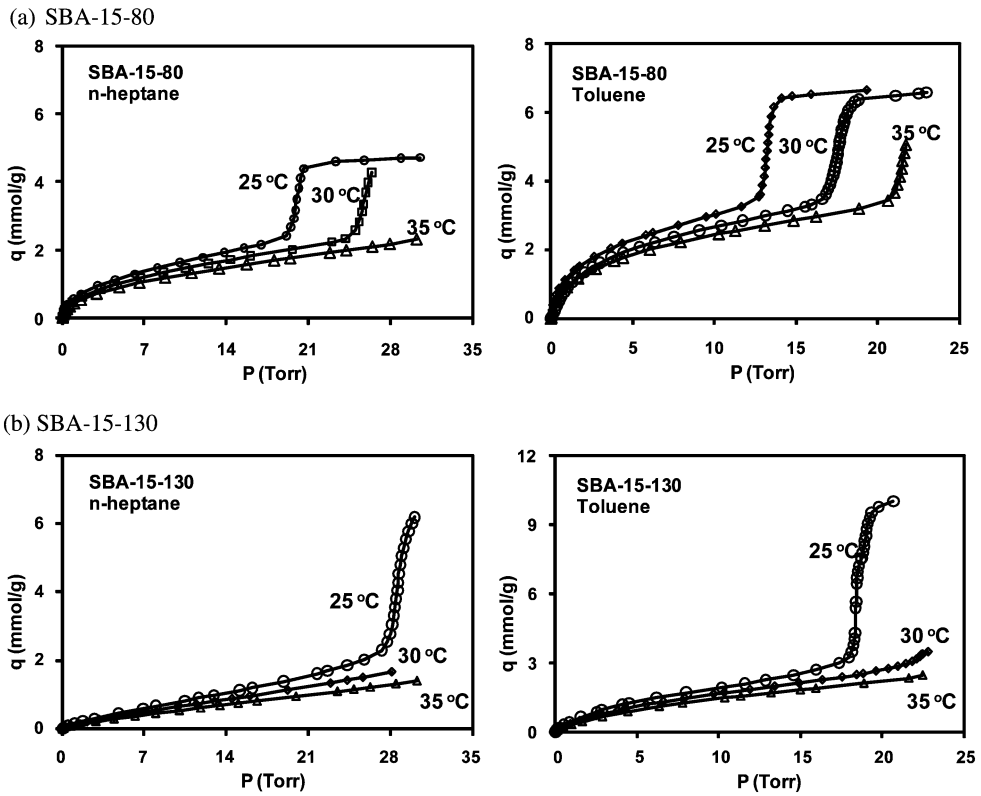

Fig. 2 Adsorption isotherms of n-heptane and toluene on (**a**) SBA-15-80 and (**b**) SBA-15-130 at various temperatures

atures are shown in Fig. 2. Capillary condensation of hydrocarbons in the mesopore channels (corresponding to the influx point on isotherm) were observed for all isotherms involving SBA-15-80 sample, except for n-heptane at 35°C. On the other hand, for SBA-15-130, only the isotherms measured at 25°C showed capillary condensations. The absence of capillary condensation phenomena for some isotherms was due to the limited relative pressure range that was possible to obtain from the experimental apparatus used in this study. Similar to nitrogen adsorption isotherm data at 77 K, adsorption equilibrium amounts of hydrocarbons in SBA-15-130 are smaller compared to those in SBA-15-80 below the onset of capillary condensation. However, after capillary condensation, the former are higher than the latter at 25°C. Evidently, the ultimate adsorption equilibrium amounts are determined by the total pore volume rather than specific surface area of materials. It can also be observed from Fig. 2 that the adsorption capacities of toluene are systematically higher than n-heptane on these two adsorbents. This is consistent with our previous results (Vinh-Thang et al. 2005a).

All ZLC results were obtained under sorbate partial pressure that would not result in capillary condensation in the primary mesopores. Therefore, in order to theoretically predict single component and binary ZLC results under non-linear conditions, the adsorption equilibrium data below the onset of capillary condensation at all temperatures for n-heptane and toluene were simultaneously fitted by the Langmuir isotherm model ($q_i = \frac{q_s b_i p_i}{1+b_i p_i}$) using non-linear regression method. The fitting curves are shown as the solid lines in Fig. 3. Apparently, the experimental data were reasonably represented by this model. The adsorption equilibrium parameters are compiled in Table 2. This table also includes the isosteric heats of adsorption (ΔH_{ads}, kJ/mol) of the two hydrocarbons on both SBA-15 samples at low sorbate load-

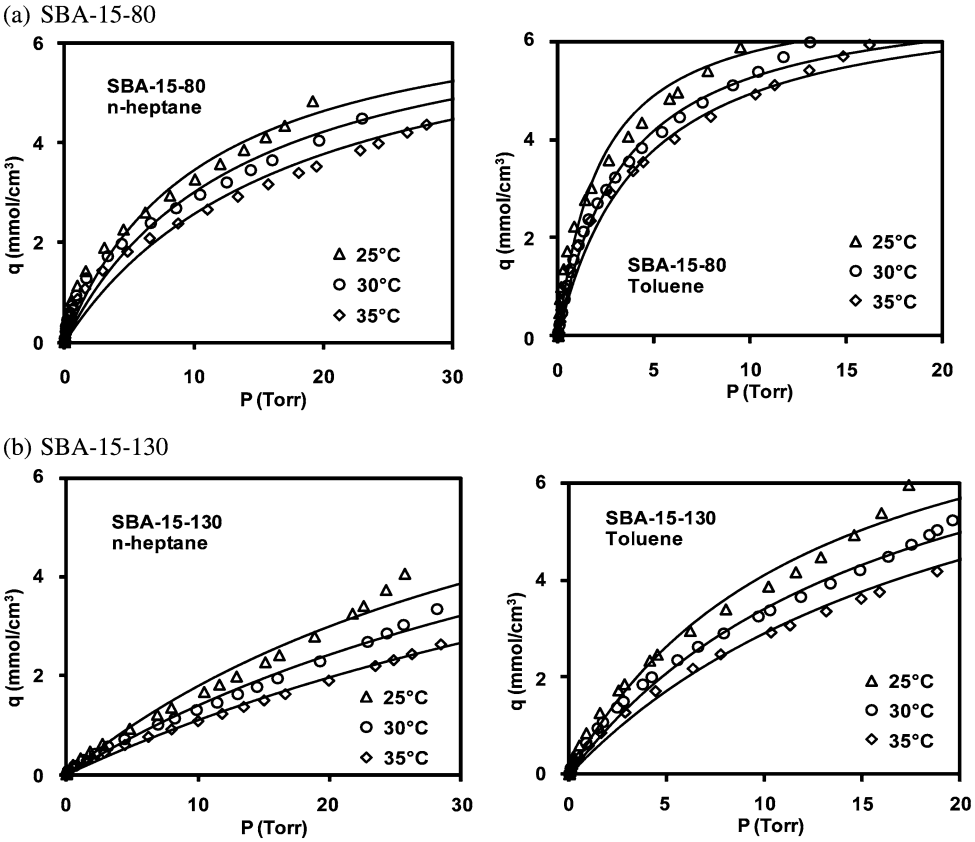

Fig. 3 Experimental (*symbols*) and Langmuir fittings (*solid lines*) of adsorption isotherms (data prior to the onset of capillary condensation): (**a**) SBA-15-80 and (**b**) SBA-15-130

ings evaluated from the temperature dependence of adsorption data using the Clausius-Clapeyron equation. The magnitudes of isosteric heats of adsorption for the two SBA-15 samples are in the order toluene > n-heptane, and SBA-15-80 has higher isosteric heats of adsorption for the two hydrocarbons than SBA-15-130. These isosteric heats of adsorption at low sorbate loadings are slightly lower in comparison with our reported results (Vinh-Thang et al. 2005a). This can be ascribed to the relatively smaller micropore volumes of the two SBA-15 samples used in this study compared to the samples used in our earlier study.

4.3 Diffusion results

4.3.1 Singe component ZLC in the linear range

Experimental ZLC desorption curves for n-heptane and toluene in SBA-15-80 and SBA-15-130 are presented in Fig. 4. The desorption data in the long time region were fitted using (6)–(8) shown in the theoretical section. The extracted values of limiting diffusional time constant (D_{oi}/R^2) are listed in Table 2. The table also lists the values of limiting diffusivity and activation energy, which were obtained from particle size analysis using SEM micrographs, and Arrhenius-type relationship, respectively. As can be seen from Table 2, n-heptane exhibits higher limiting diffusivity values than toluene, which is opposite to the trend of their critical molecular sizes (toluene: 0.585 nm; n-heptane: 0.430 nm). Furthermore, the limiting diffusivities for probe molecules increase with the decrease of the relative content of micropore volume in both samples. The limiting diffusivities for n-heptane in SBA-15-80 and SBA-15-130 were also found comparable to those measured on SBA-15 samples with larger micropore volumes (Vinh-Thang et al. 2005b).

The apparent activation energy values of n-heptane and toluene are higher in SBA-15-80 than SBA-15-130. They are somewhat lower in comparison with those for saturated hydrocarbons (C-5 to C-10 carbon range) diffusion in silicalite, and benzene and ethyl-benzene diffusion in MFI zeolites (Kärger and Ruthven 1992), respectively. However, they are much smaller than the values of the limiting heat of adsorption for n-heptane and toluene in two SBA-15 samples (see Table 2). According to the parallel diffusion model proposed by Vinh-Thang et al. (2006a, 2006b), which considers combination of mesopore diffusion in main channels with an activated diffusion in the intrawall structure of the bi-porous materials, the limiting (effective) diffusivity is defined by the following expression,

$$D_{oi} = \frac{\varepsilon_p D_{\text{meso}}}{\tau_1(1-\varepsilon_p)K} + \frac{D_{\text{intraw}}}{\tau_2} \tag{15}$$

where D_{meso} and D_{intraw} ($= f(D_{\text{iwmicro}}, D_{\text{iwmeso}}, D_{\text{ws}})$) are diffusivities in the primary mesopores and intrawall pore

Table 2 Kinetic and equilibrium parameters and limiting heat of adsorption of n-heptane and toluene for SBA-15 samples

Sample	Sorbate	Kinetic parameters			E (kJ/mol)
		T (°C)	D_{0i}/R^2 (s^{-1})	D_{0i} (m^2/s)	
SBA-15-80	n-Heptane	25	4.29×10^{-4}	8.69×10^{-15}	12.6
(9.0 μm)		40	5.41×10^{-4}	1.10×10^{-14}	
		55	6.82×10^{-4}	1.38×10^{-14}	
	Toluene	25	2.58×10^{-4}	5.22×10^{-15}	17.7
		55	4.56×10^{-4}	9.23×10^{-15}	
		85	8.56×10^{-4}	1.73×10^{-14}	
SBA-15-130	n-Heptane	25	6.27×10^{-4}	2.07×10^{-14}	11.8
(11.5 μm)		40	7.91×10^{-4}	2.62×10^{-14}	
		55	9.67×10^{-4}	3.20×10^{-14}	
	Toluene	25	3.05×10^{-4}	1.01×10^{-14}	13.2
		40	3.92×10^{-4}	1.30×10^{-14}	
		55	4.97×10^{-4}	1.64×10^{-14}	
		Langmuir parameters and limiting isosteric heat of adsorption			
		T (°C)	b ($Torr^{-1}$)	q_s ($mmol/cm^3$)	$-\Delta H_{ads}$ (kJ/mol)
SBA-15-80	n-Heptane	25	9.56×10^{-2}	70	60
		30	7.40×10^{-2}		
		35	5.70×10^{-2}		
	Toluene	25	4.59×10^{-1}		71
		30	2.92×10^{-1}		
		35	2.34×10^{-1}		
SBA-15-130	n-Heptane	25	2.42×10^{-2}	9.2	48
		30	1.79×10^{-2}		
		35	1.35×10^{-2}		
	Toluene	25	8.07×10^{-2}		59
		30	5.89×10^{-2}		
		35	4.62×10^{-2}		

structures, respectively; D_{intraw} is a complex function of surface diffusivity along surface of the primary mesopore walls (D_{ws}), in addition to micropore and secondary mesopore diffusivities (D_{iwmicro} and D_{ws}) in the intrawall porous structure, as indicated in the parallel diffusion model mentioned above; τ_1 and τ_2 are mesopore tortuosity and intrawall pore tortuosity, respectively; ε_p is particle mesoporosity. It is evident that the temperature dependence of D_{oi} is primarily related to the temperature dependence of K, and D_{intraw}. Activation energies for D_{intraw} are expected to have low to modest values in comparison to the limiting heats of adsorption. If the mass transfer process is driven by diffusion in primary mesopores, the effective activation energy would be approaching limiting heat of adsorption, according to the temperature dependency of Henry's law constant (K), from the first term of (15). On the other hand, if the intrawall diffusion is governing the mass transfer then the effective activation energy would be approaching diffusion activation energy in micropores of the intrawall structure, e.g., the second term in (15). Based on these arguments, it is plausible to associate the transport properties of n-heptane and toluene, at the temperature range used in this study, to the micropore and/or secondary mesopore transport mechanism in the intrawall porous structure of the SBA samples, which is characterized by relatively low activation energies, i.e., the second term of (15). Moreover, if the relative micropore content of material is higher, the relative contribution of intrawall micropore diffusivity to the effective diffusivity is larger, according to the parallel diffusion model, indicating that the second term of (15) is more significant to the overall (effective) diffusivity.

4.3.2 Singe component ZLC in the nonlinear range

Single component n-heptane and toluene ZLC in SBA-15-80 and SBA-15-130 were measured for a step reduction of

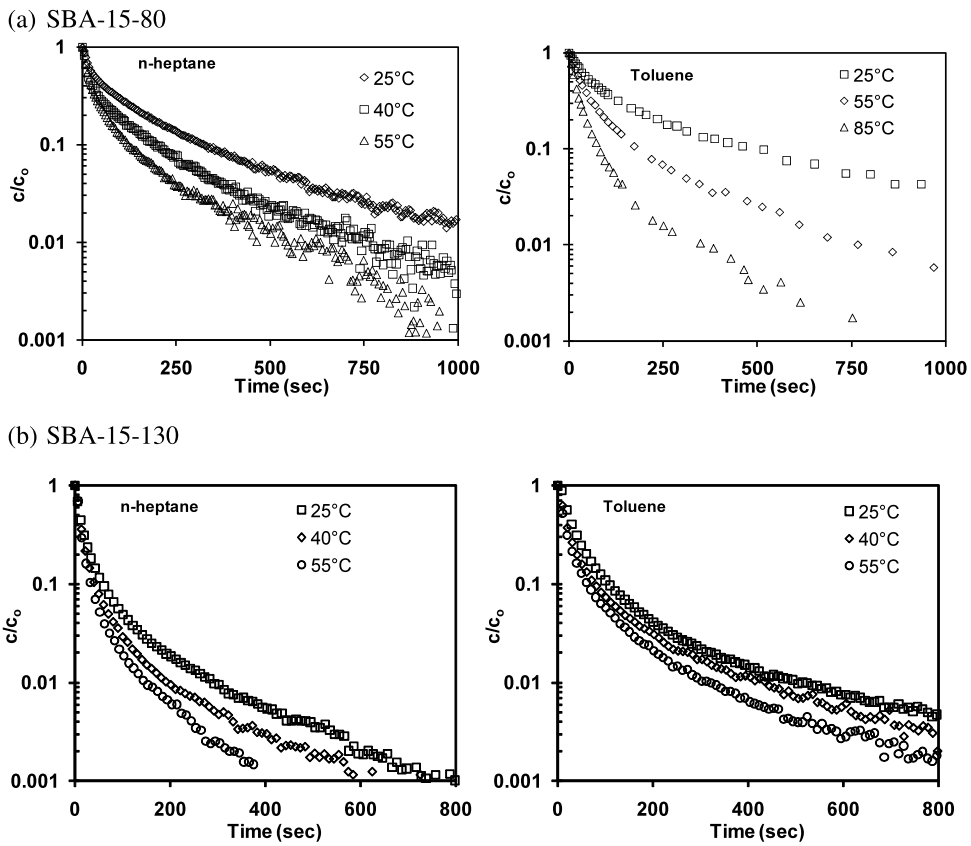

Fig. 4 Experimental ZLC curves for n-heptane and toluene obtained at the low concentration levels and the purge flow rate of 30 cm^3/min: (**a**) SBA-15-80 and (**b**) SBA-15-130

partial pressure from 10 to 0 Torr, and 5 to 0 Torr, respectively. The model predictions by (3), (4), (9), (10) using kinetic and equilibrium parameters in Table 2 are compared with experimental ZLC results in Fig. 5. In the model prediction, the volume of SBA-15 particle, v_s, was estimated according to the following equation,

$$v_s = \frac{m}{\rho_s} + m v_t \tag{16}$$

where m is weight of dry sample; ρ_s is sample pore wall density assumed to be equal to that of amorphous silica (2.2 g/cm^3); v_t is total pore volume of sample in Table 1.

As can be seen from Fig. 5, except for some deviation in the short time region of desorption profiles that may be due to the apparatus effect, the theoretical model provides an overall quantitative prediction of the experimental results in both SBA-15 samples. This verifies the validity of theoretical model that is based on GMS theory.

4.3.3 Binary counter-diffusion ZLC

Figure 6 shows experimental binary CCZLC results for n-heptane and toluene in two SBA-15 samples at low concentrations and 55°C. Single component NZLC results for n-heptane and toluene are also displayed in the same figure for comparison. It is evident that NZLC and CCZLC results for toluene in both SBA-15 samples essentially overlap, indicating that the diffusivity of toluene is not affected by the presence of n-heptane. However, CCZLC results for n-heptane purged by toluene at two different partial pressures (0.01 and 2 Torr) show retarding effects of toluene on n-heptane diffusion. The slopes of the long time asymptotes, which relate to the magnitude of n-heptane diffusivity, are lesser for CCZLC compared to the NZLC results, showing more pronounced effects, as the partial pressure of toluene (purge gas) is increased. This obviously suggests that the diffusion rate of n-heptane is somewhat slowed by the counter-flux of toluene. The observed phenomenon can be explained by the mechanism of single-file diffusion of probe molecules in the one-dimensional materials (Iliyas et al. 2008). As discussed in Sect. 4.3.1 the transport of n-heptane and toluene is controlled by the micropores in SBA-15 materials. These microporous channels exist in the walls of ordered primary mesoporous structure, and are distributed in a disordered way. Most of them, together with secondary-mesopores, are considered to provide connectivity between the primary mesopores (Vinh-Thang et al. 2005b). They are considered one-dimensional channels interconnecting primary mesopores. However, they do not seem to be large enough for n-heptane and toluene molecules to cross one another. When the adsorbed n-heptane molecule is desorbed by toluene, the slowly moving toluene molecule obstructs

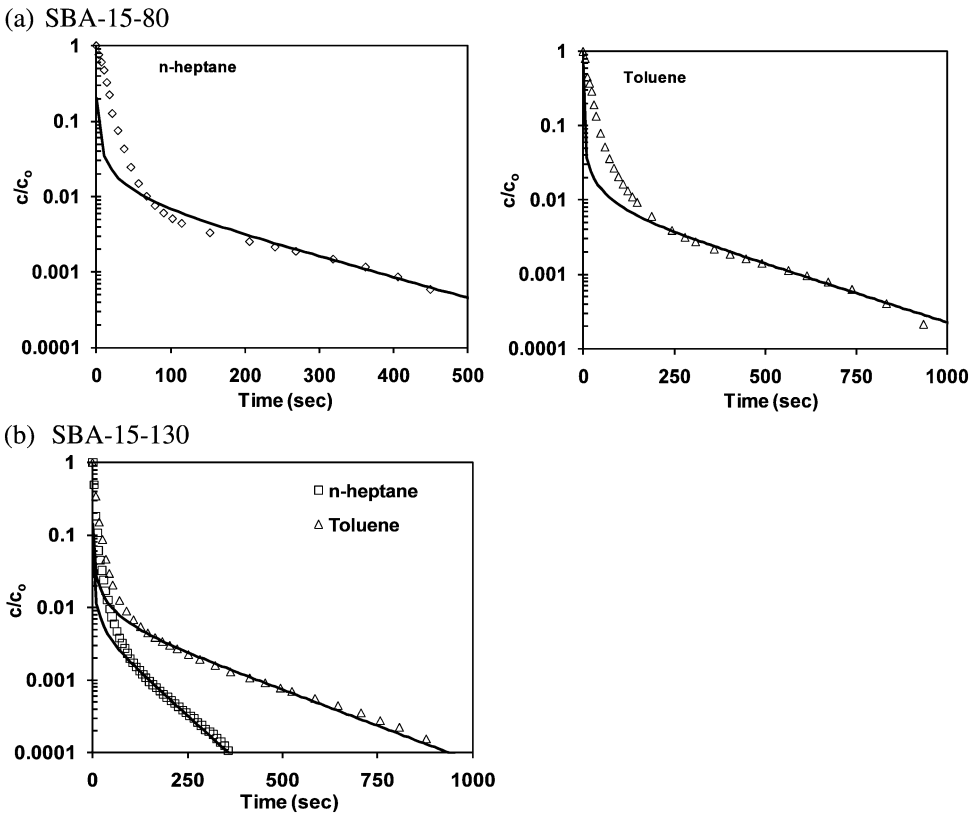

Fig. 5 Experimental (*symbols*) and theoretical (*solid lines*) ZLC curves for n-heptane (10 Torr) and toluene (5 Torr) obtained at the purge flow rate of 25 cm^3/min and 55°C: (**a**) SBA-15-80 and (**b**) SBA-15-130

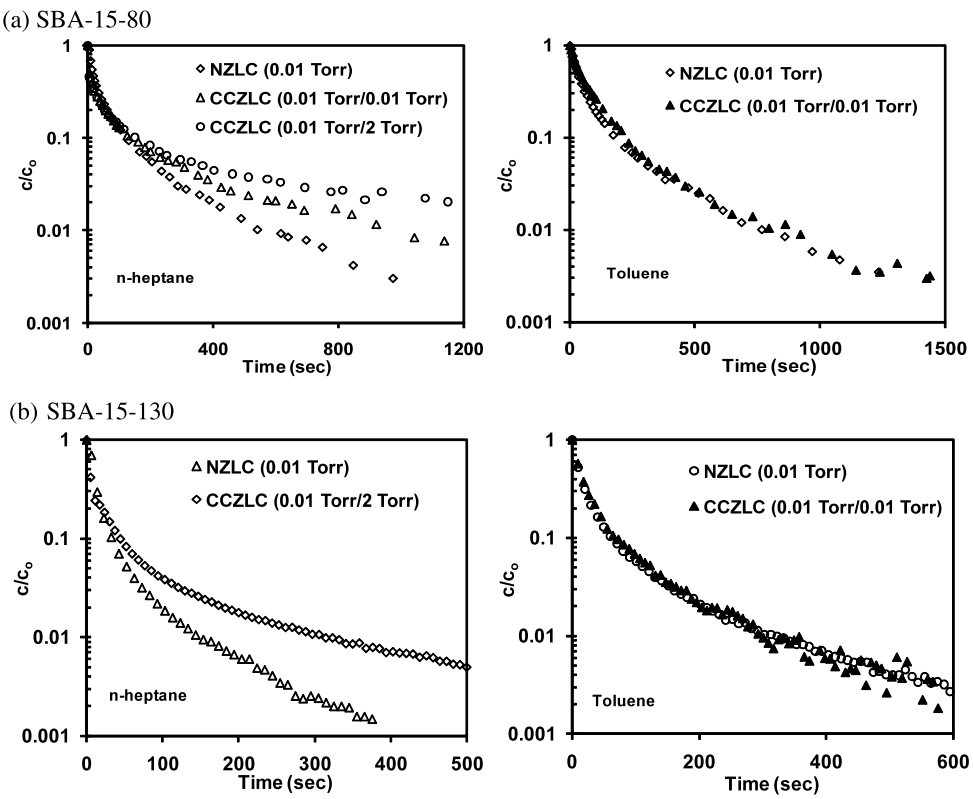

Fig. 6 Experimental ZLC desorption results for n-heptane and toluene in (**a**) SBA-15-80 and (**b**) SBA-15-130 at the purge flow rate of 30 cm^3/min and 55°C. In the figure, NZLC—single component n-heptane or toluene ZLC measured at low concentration (0.01 Torr partial pressure); CCZLC—for n-heptane counter diffusion run, sample is equilibrated at 0.01 Torr n-heptane and then desorbed with 0.01 or 2 Torr toluene in He, and for toluene counter diffusion run, sample is equilibrated at 0.01 Torr toluene and then desorbed with 0.01 Torr n-heptane in He

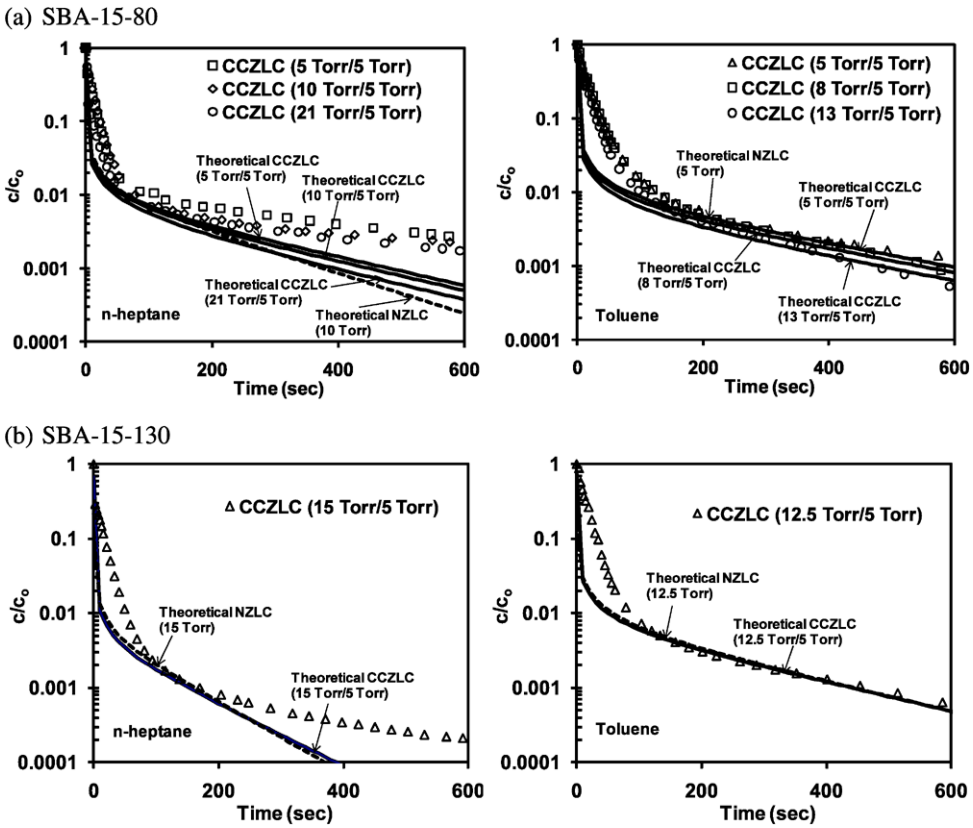

Fig. 7 Experimental (*symbols*) and theoretical (*solid lines*) CCZLC desorption results for n-heptane and toluene in (**a**) SBA-15-80 and (**b**) SBA-15-130 at the purge flow rate of 25 cm^3/min and 55°C. Additional theoretical NZLC desorption curves (*dotted lines*) for n-heptane and toluene are also shown on each diagram for comparisons. In the figure, CCZLC—for n-heptane counter diffusion run, sample is equilibrated with n-heptane at various pressures and then desorbed with 5 Torr toluene in He, and for toluene counter diffusion run, sample is equilibrated with toluene at various pressures and then desorbed with 5 Torr n-heptane in He

the pathways of microporous channels, thus controlling the transport process by slowing down the faster species, e.g., n-heptane, close to its own diffusion rate. On the other hand, when the adsorbed toluene molecule is purged (desorbed) by low n-heptane concentration, the smaller n-heptane molecule moves faster than toluene in the micropores (no obstruction) rendering the diffusion rate of toluene to stay unaffected. Therefore, based on the critical molecular diameters of n-heptane and toluene and considering single-file diffusion mechanism, the average size of micropores in the two SBA-15 samples can be estimated to be smaller than 1.015 nm, which corresponds to the sum of the probe molecules' diameters.

Valiullin et al. (2005) and Dvoyashkin et al. (2009) applied pulsed field gradient NMR method to study self-diffusion of organic molecules in mesoporous materials. They concluded that surface diffusion dominated the transport process, and observed that the distribution of the adsorptive energies would lead to a complex interplay between selective adsorption and pathway blockage along the pore space, which could slow down the diffusion of probe molecules. Our observations from binary CCZLC for n-heptane and toluene in the SBA-15 samples are similar to those reported in the literature (Baertsch et al. 1996; Brandani et al. 2000a, 2000b; Qureshi and Wei 1990a, 1990b). Baertsch et al. (1996) observed from permeation measurements with a silicalite-zeolite membrane that o-xylene slowed down the permeation of p-xylene to a greater extent than expected, if the permeation was based on single-component diffusion only. They associated their observations to single-file diffusion through the silicalite pores. Brandani et al. (2000a, 2000b) studied counter diffusion of benzene/p-xylene, benzene/o-xylene and p-xylene/o-xylene in silicalite using ZLC technique. They found that the slowly diffusing o-xylene obstructed the desorption of the faster moving benzene and/or p-xylene, while the desorption of benzene was not affected by the counter-flux of p-xylene since both benzene and p-xylene exhibited similar diffusivities. Qureshi and Wei (1990a, 1990b) measured co- and counterdiffusion of benzene and toluene in ZSM-5 crystals and found that their results were interpreted well with a single-file diffusion model.

In order to further investigate the binary diffusion of n-heptane and toluene in SBA-15 materials, ZLC desorption measurements from samples initially saturated with n-heptane/toluene at various partial pressures ranging from 5 to 21 Torr, followed by purging with helium stream containing 5 Torr toluene/n-heptane at a flow rate of 25 cm^3/min were carried out. The CCZLC results for the two SBA-15 samples at 55°C are presented in Fig. 7. It can be observed that the long time asymptotes are generally parallel but the intercepts shift down with the increasing saturation pressures. The change in intercept is due to the increasing curvature of adsorption isotherms of n-heptane/toluene at

higher pressures. Figure 7 also displays the theoretical CCZLC curves (solid lines) calculated from the proposed binary model (3), (4), (11)–(14), using independently measured single component equilibrium and kinetic parameters shown in Table 2, as well as theoretical NZLC curves (dotted lines) for n-heptane and toluene at one pressure calculated from single component model (3), (4), (9), (10). Apparently, theoretical curves for toluene calculated from both CCZLC and NZLC models almost overlap, clearly indicating that the desorption of toluene is not influenced by the presence of n-heptane. The theoretical models deviate only in the prediction of experimental CCZLC results for toluene in the short time region, but they predict the long time asymptotes reasonably well. On the other hand, both binary CCZLC and single component NZLC models fail to predict CCZLC results for n-heptane in the entire time range, although the former model shows somewhat better prediction than the latter e.g., smaller slopes of the long time asymptotes, which are closer to the experimental results. Both models require smaller diffusion time constant values of n-heptane to match the experimental long time asymptotes. These results confirm that the diffusion of n-heptane is affected and retarded by the counter-flux of toluene. We therefore conclude that, in contrast to the toluene/n-heptane system, neither of the simple diffusion models cannot properly represent the behavior of the n-heptane/toluene system.

5 Conclusions

In this study, diffusion of single component and binary n-heptane and toluene in two silica SBA-15 materials was investigated by the ZLC technique. It was established that diffusion of n-heptane and toluene is controlled by micropores in the porous structure of intra-walls, and diffusivity values increase with the decrease of micropore content. Results from counter-current ZLC measurements for binary n-heptane and toluene revealed that the faster diffusing n-heptane is slowed by the counter-flux of slowly moving toluene, while the diffusion of toluene is unaffected with the existence of n-heptane. The observed behavior can be explained by the single-file diffusion of probe molecules in the microporous channels. The observation also implies that a great part of micropores in SBA-15 samples are of size less than 1.01 nm.

The experimental ZLC results of single component n-heptane and toluene in the nonlinear range are reasonably predicted by the theoretical model derived from GMS theory. The theoretical model for the binary system also provides quantitative prediction of ZLC desorption of toluene by the counterdiffusion of n-heptane using independently measured single-component kinetic and equilibrium parameters, while it largely deviates in the prediction of n-heptane data by the counterdiffusion of toluene. Such deviation is due to the slowing effect of toluene on the diffusion rate of n-heptane and requires further investigation, e.g., single-file diffusion measurements of the probe molecules using the ZLC method.

Acknowledgements This project was supported by the Natural Science and Engineering Research Council of Canada (NSERC). Special thanks are due to Professor Serge Kaliaguine, Laval University, Canada for providing the two SBA-15 samples, and Mr. Shum Kai Lau for taking a part in the ZLC measurements.

References

Baertsch, C.D., Funke, H.H., Falconer, J.L., Noble, R.D.: Permeation of aromatic hydrocarbon vapors through silicalite-zeolite membranes. J. Phys. Chem. **100**, 7676–7679 (1996)

Brandani, S., Jama, M., Ruthven, D.M.: Diffusion, self-diffusion and counter-diffusion of benzene and p-xylene in silicalite. Micropor. Mesopor. Mater. **35–36**, 283–300 (2000a)

Brandani, S., Jama, M., Ruthven, D.M.: Counterdiffusion of p-xylene/benzene and p-xylene/o-xylene in silicalite studied by the zero-length column technique. Ind. Eng. Chem. Res. **39**, 821–828 (2000b)

Brandani, S., Jama, M., Ruthven, D.M.: ZLC measurements under non-linear conditions. Chem. Eng. Sci. **55**, 1205–1212 (2000c)

Choi, M., Heo, W., Kleitz, F., Ryoo, R.: Facile synthesis of high quality mesoporous SBA-15 with enhanced control of the porous network connectivity and wall thickness. Chem. Commun. **12**, 1340–1341 (2003)

Dvoyashkin, M., Khokhlov, A., Naumov, S., Valiullin, R.: Pulsed field gradient NMR study of surface diffusion in mesoporous adsorbents. Micropor. Mesopor. Mater. **125**, 58–62 (2009)

Eić, M., Ruthven, D.M.: A new experimental-technique for measurement of intracrystalline diffusivity. Zeolites **8**, 40–45 (1988)

Galarneau, A., Cambon, H., Di Renzo, F., Ryoo, R., Choi, M., Fajula, F.: Microporosity and connections between pores in SBA-15 mesostructured silicas as a function of the temperature of synthesis. New J. Chem. **27**, 73–79 (2003)

Iliyas, A., Eić, M., Zahedi-Niaki, M.H., Vasenkov, S.: Toward observation of single-file diffusion using the tracer zero-length column method. J. Phys. Chem. B **112**, 3821–3825 (2008)

Kärger, J., Ruthven, D.M.: Diffusion in Zeolites and Other Microporous Materials. Wiley, New York (1992)

Krishna, R.: A unified approach to the modeling intraparticle diffusion in adsorption processes. Gas Sep. Purif. **7**, 91–104 (1993)

Kruk, M., Jaroniec, M., Ko, C.H., Ryoo, R.: Characterization of the porous structure of SBA-15. Chem. Mater. **12**, 1961–1968 (2000)

Kruk, M., Jaroniec, M., Sayari, A.: Application of large pore MCM-41 molecular sieves to improve pore size analysis using nitrogen adsorption measurements. Langmuir **13**, 6267–6273 (1997)

Newalkar, B.L., Choudary, N.V., Kumar, P., Komarneni, S., Bhat, T.S.G.: Exploring the potential of mesoporous silica, SBA-15, as an adsorbent for light hydrocarbon separation. Chem. Mater. **14**, 304–309 (2002)

Qureshi, W.R., Wei, J.: One- and two-component diffusion in zeolite ZSM-5 I. theoretical. J. Catal. **126**, 126–146 (1990a)

Qureshi, W.R., Wei, J.: One- and two-component diffusion in zeolite ZSM-5 II. experimental. J. Catal. **126**, 147–172 (1990b)

Ravikovitch, P.I., Neimark, A.V.: Characterization of micro- and mesoporosity in SBA-15 materials from adsorption data by the NLDFT method. J. Phys. Chem. B **105**, 6817–6823 (2001)

Rioux, R.M., Song, H., Hoefelmeyer, J.D., Yang, P., Somorjai, G.A.: High-surface-area catalyst design: synthesis, characterization, and reaction studies of platinum nanoparticles in mesoporous SBA-15 silica. J. Phys. Chem. B **109**, 2192–2202 (2005)

Round, G.F., Habgood, H.W., Newton, R.: Diffusion in a binary adsorbed phase. Sep. Sci. **1**, 219–227 (1966)

Sun, Y., Han, Y., Yuan, L., Ma, S., Jiang, D., Xiao, F.S.: Microporosity in ordered mesoporous aluminosilicates characterized by catalytic probing reactions. J. Phys. Chem. B **107**, 1853–1857 (2003)

Valiullin, R., Kortunov, P., Kärger, J., Timoshenko, V.: Surface self-diffusion of organic molecules adsorbed in porous silicon. J. Phys. Chem. B **109**, 5746–5752 (2005)

Vignes, A.: Diffusion in binary solutions. Ind. Eng. Chem. Fundamental **5**, 189–199 (1966)

Vinh-Thang, H., Huang, Q.L., Eić, M., Trong-On, D., Kaliaguine, S.: Adsorption of C7 hydrocarbons on biporous SBA-15 mesoporous silica. Langmuir **21**, 5094–5101 (2005a)

Vinh-Thang, H., Huang, Q.L., Eić, M., Trong-On, D., Kaliaguine, S.: Structure and diffusion characterization of SBA-15 materials. Langmuir **21**, 2051–2057 (2005b)

Vinh-Thang, H., Huang, Q.L., Eić, M., Trong-On, D., Kaliaguine, S.: Effect of the intrawall microporosity on the diffusion characterization of bi-porous SBA-15 materials. In: Conner, C., Fraissard, J. (eds.) Fluid Transport in Nanoporous Material. NATO Sci. Series, vol. 219, pp. 591–602. Springer, Berlin (2006a)

Vinh-Thang, H., Huang, Q.L., Ungureanu, A., Eić, M., Trong-On, D., Kaliaguine, S.: Structural and diffusion characterizations of steam-stable mesostructured zeolitic UL-ZSM-5 materials. Langmuir **22**, 4777–4786 (2006b)

Zhao, D.Y., Huo, Q., Feng, J., Chmelka, B.F., Stucky, G.D.: Nonionic triblock and star diblock copolymer and oligomeric surfactant syntheses of highly ordered, hydrothermally stable, mesoporous silica structures. J. Am. Chem. Soc. **120**, 6024–6036 (1998)

Zhao, J.W., Gao, F., Fu, Y., Wan, J., Yang, P., Zhao, D.Y.: Biomolecule separation using large pore mesoporous SBA-15 as a substrate in high performance liquid chromatography. Chem. Commun. 752–753 (2002)